Developmental Cell
Article

# *Arabidopsis* Serrate Coordinates Histone Methyltransferases ATXR5/6 and RNA Processing Factor RDR6 to Regulate Transposon Expression

Zeyang Ma,[1,2] Claudia Castillo-González,[1,2] Zhiye Wang,[1,2] Di Sun,[1,2] Xiaomei Hu,[1,2] Xuefeng Shen,[1,2,3] Magdalena E. Potok,[4] and Xiuren Zhang[1,2,5,*]
[1]Department of Biochemistry and Biophysics, Texas A&M University, College Station, TX 77843, USA
[2]Institute for Plant Genomics and Biotechnology, Texas A&M University, College Station, TX 77843, USA
[3]College of Agriculture, South China Agricultural University, Guangzhou 510642, China
[4]Department of Molecular, Cell and Developmental Biology, University of California at Los Angeles, Los Angeles, CA 90095, USA
[5]Lead Contact
*Correspondence: xiuren.zhang@tamu.edu
https://doi.org/10.1016/j.devcel.2018.05.023

## SUMMARY

**Serrate (SE) is a key component in RNA metabolism. Little is known about whether and how it can regulate epigenetic silencing. Here, we report histone methyltransferases ATXR5 and ATXR6 (ATXR5/6) as novel partners of SE. ATXR5/6 deposit histone 3 lysine 27 monomethylation (H3K27me1) to promote heterochromatin formation, repress transposable elements (TEs), and control genome stability in *Arabidopsis*. SE binds to ATXR5/6-regulated TE loci and promotes H3K27me1 accumulation in these regions. Furthermore, SE directly enhances ATXR5 enzymatic activity *in vitro*. Unexpectedly, *se* mutation suppresses the TE reactivation and DNA re-replication phenotypes in the *atxr5 atxr6* mutant. The suppression of TE expression results from triggering RNA-dependent RNA polymerase 6 (RDR6)-dependent RNA silencing in the *se atxr5 atxr6* mutant. We propose that SE facilitates ATXR5/6-mediated deposition of the H3K27me1 mark while inhibiting RDR6-mediated RNA silencing to protect TE transcripts. Hence, SE coordinates epigenetic silencing and RNA processing machineries to fine-tune the TE expression.**

## INTRODUCTION

TEs make up a substantial portion of most eukaryotic genomes. Due to potentially deleterious effects, TEs usually undergo transcriptional gene silencing (TGS) (Matzke and Mosher, 2014; Sienski et al., 2012). However, TEs can also contribute to the regulatory variation of endogenous gene expression and impact the organism's fitness in certain circumstances, like environmental stresses (Iwasaki and Paszkowski, 2014; Lisch, 2013; Makarevitch et al., 2015). Hence, the reactivation and expression of TEs need to be tightly regulated to meet various functional needs. One mechanism to control TE expression is through chromatin modifications, such as histone methylation (Tan et al., 2011). H3K27 methylations, present in mono-, di-, and trimethylated states (H3K27me1/2/3), are repressive marks (Deal and Henikoff, 2011). In animals, the polycomb repressive complex 2 (PRC2) accounts for H3K27me3 but also affects all forms of H3K27 methylation (Jiao and Liu, 2015). In *Arabidopsis*, H3K27me2/3 are primarily deposited by PRC2 (Liu et al., 2010), whereas H3K27me1 is predominantly catalyzed by ATXR5/6 (Jacob et al., 2009). H3K27me2/3 are repressive marks in the facultative heterochromatin and are responsible for the repression of many coding genes (Margueron and Reinberg, 2011). In contrast, H3K27me1 is mainly enriched at heterochromatin where TEs and repetitive sequences are located. Loss of ATXR5/6 causes a reduction in H3K27me1, transcriptional activation of TEs, and a genomic instability defect termed DNA re-replication (Jacob et al., 2009, 2010).

Regulation of endogenous loci also involves cooperation between the TGS and posttranscriptional gene silencing (PTGS) pathways. For examples, Dicer-like 1 (DCL1), a core enzyme in the plant microprocessor (Zhu et al., 2013), participates in silencing of a subset of transposons through positive regulation of DNA methylation (Laubinger et al., 2010). Second, DCL1-dependent microRNAs (miRNAs) can target TE transcripts, which are canonically repressed by the TGS pathway, to produce epigenetically activated small interfering RNAs (easiRNAs) via RNA-dependent RNA polymerase 6 (RDR6) and DCL4 (Creasey et al., 2014). The easiRNAs not only function through RNA-induced silencing complexes (RISC) to clear transcripts of reactivated TEs but also affect the DNA methylation status at the corresponding loci. Third, AGO2 and DCL2, among other PTGS components, can direct DNA methylation by priming an RNA Polymerase II–RDR6-engaged RNA-directed DNA methylation (RdDM) pathway (Matzke et al., 2015). In addition, cap-binding complex (CBC), best known for its roles in RNA processing, interacts with H3K4me3 and H3K36me3 methyltransferases complexes. The CBC and histone methyltransferases function interdependently to regulate the activation of gene expression and efficient pre-mRNA splicing (Li et al., 2016).

SE, an ortholog of the mammalian Ars2, is known as an essential component of the plant microprocessor, acting with DCL1 and HYL1 to produce miRNAs (Gruber et al., 2009; Sabin et al., 2009; Yang et al., 2006). SE also participates in splicing

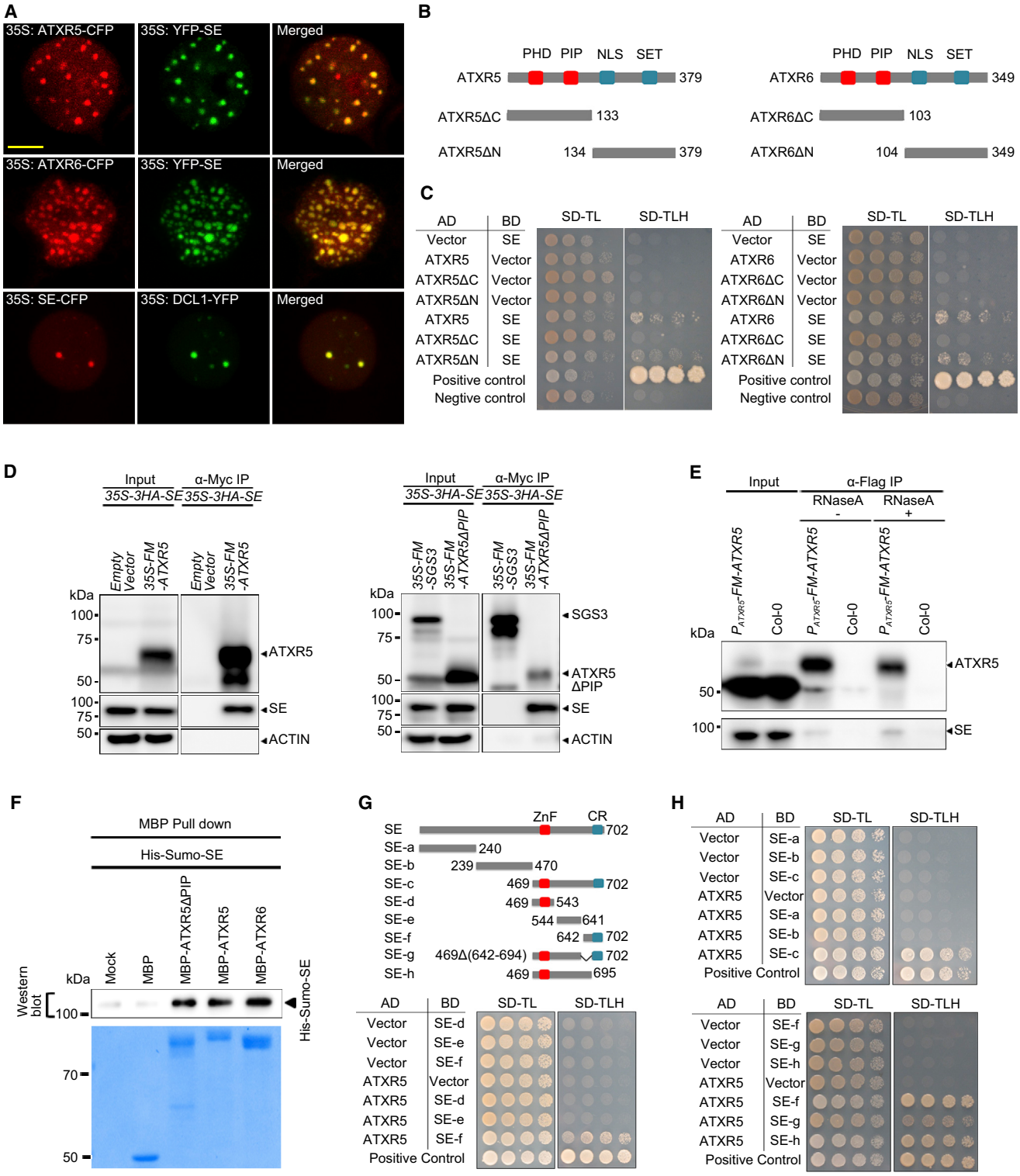


**Figure 1. ATXR5 Is a *Bona Fide* Partner of SE in *Arabidopsis***

(A) Confocal microscopy image shows co-localization of *35S-YFP-SE* with *35S-ATXR5/6-CFP* and *35S-DCL1-YFP* with *35S-SE-CFP* in *N. benthamiana*. Bar, 5 μM.

(B) Schematic diagram of the full-length and truncated ATXR5/6 used in the Y2H assay. NLS, nuclear localization signal; SET, su(var) E(Z) trithorax domain.

(C–F) Validation of SE and ATXR5/6 interaction by Y2H assays (C), co-IP in *N. benthamiana* (D) and in *Arabidopsis* (E), and *in vitro* pull-down assays (F). In (C), AD, GAL4 activation; BD, DNA-binding domain. SD, synthetic dropout medium. −TLH, minus Trp, Leu, and His. Positive control, pGADT7-βC1 and pGBKT7-NtRFP.

*(legend continued on next page)*

of pre-mRNA, especially in the processing of the first introns (Laubinger et al., 2008; Raczynska et al., 2014). This function is fulfilled presumably through the interaction with the CBC (Hallais et al., 2013; Laubinger et al., 2008; Raczynska et al., 2014). Previous studies show that the expression of some TEs and long intergenic noncoding RNAs (lncRNAs) are also affected in *se* mutants (Laubinger et al., 2010; Liu et al., 2012), raising the possibility that SE might function in transcriptional regulation. Indeed, *Ars2* has recently been reported as a new transcription factor in mammals, directly participating in the transcriptional regulation of the pluripotency factor *Sox2* (Andreu-Agullo et al., 2012). However, whether and how SE regulates epigenetic silencing globally has not been explored.

In this study, we identified ATXR5/6 as components of SE in plants. We found that SE is essential for the maintenance of ATXR5/6-catalyzed H3K27me1 *in vivo* and this role is independent of its canonical function in RNA metabolism. SE protein associates with the ATXR5/6-regulated TE loci *in vivo* and directly enhances ATXR5 enzymatic activity *in vitro*. Surprisingly, although SE is a positive regulator of H3K27me1 repressive mark, the *se* mutation does not generally activate the expression of ATXR5/6-regulated TE loci and DNA re-replication. Rather, the *se* mutation suppresses the transcriptional activation of TEs and DNA re-replication phenotypes in the *atxr5 atxr6* mutant. We also found that the suppression of TE expression in the *se-2 atxr5 atxr6* mutant results from triggering the RDR6-dependent RNA silencing. Thus, SE plays dual roles in regulating TE expression at both the TGS and PTGS levels. Whereas SE promotes ATXR5/6-mediated H3K27me1 deposition, this protein also protects the reactivated TE transcripts through repressing the RDR6-dependent PTGS pathway. This study provides new insight into the synchronization between the epigenetic and RNA silencing machineries to tightly control the TE expression in the eukaryotes.

## RESULTS

### ATXR5 and ATXR6 Are *Bona Fide* Partners of SE

To study the function of SE, we proposed to identify its cofactors *in vivo*. To this end, we generated *35S-Flag-4Myc(FM)-SE* transgenic plants and isolated the SE complexes by two-step immunoprecipitation (Wang et al., 2018). Mass spectrometry (MS) analysis of the immunoprecipitate recovered ATXR5 from the *FM-SE* transgenic plants but not from that of the control Col-0 (Figure S1A). ATXR5 has a genetic paralog, ATXR6, with 62.3% amino acid (aa) sequence similarity and 52.6% identity (Figure S1B). Both proteins are H3K27me1 methyltransferases and function in epigenetic silencing of TEs (Jacob et al., 2009). ATXR6 was not detected by our MS analysis, likely because *ATXR5* transcript is much more abundant than that of *ATXR6* in apex and leaf tissues (Jacob et al., 2009). Moreover, a single mutant of *atxr5*, but not *atxr6*, exhibits a defect in rRNA gene expression, which is proposed to be regulated by H3K27me1, while the *atxr5 atxr6* double mutant shows synergistic effect (Pontvianne et al., 2012), suggesting that ATXR5 predominantly contributes to certain physiological conditions. Therefore, ATXR5 methyltransferase is the focus in our study with some experiments including ATXR6.

To verify the proteomics result, we first evaluated SE and ATXR5/6 localization *in vivo* by confocal microscopy. SE and ATXR5/6 tagged with yellow fluorescent protein/cyan fluorescent protein (YFP/CFP) are localized at discrete nuclear foci, and they also showed dispersed nuclear signals when transiently expressed under the *35S* promoter in *Nicotiana (N) benthamiana* (Figure S1C). When co-expressed, YFP-SE and ATXR5/6-CFP were co-localized at nuclear speckles (Figure 1A). Notably, these speckles of ATXR5/6-CFP were different from Dicer (D) bodies, which are subcellular compartments for the plant microprocessor (Fang and Spector, 2007), suggesting unidentified functions of SE (Figure S1C). We then conducted yeast-two-hybrid (Y2H) experiments and observed SE interaction with both ATXR5 and ATXR6 (Figures 1B, 1C, and S1D), but not with PRC2 components (Figure S1D). We performed coimmunoprecipitation (co-IP) assays through transiently expressing the tested components in *N. benthamiana*, and also from $P_{ATXR5}$-*FM-ATXR5 Arabidopsis* transgenic lines. SE was coimmunoprecipitated with ATXR5 but not with the control proteins (Figure 1D). Importantly, the presence of SE in the ATXR5 IP was not abolished by RNase A treatment, suggesting that their interaction is RNA-independent *in vivo* (Figure 1E). Furthermore, *in vitro* pull-down assays showed that MBP-ATXR5 and MBP-ATXR6, but not MBP protein alone, directly interacted with SE (Figure 1F). Taken together, these results indicate that ATXR5/6 are *bona fide* partners of SE.

Next, we roughly mapped the interaction interface between ATXR5/6 and SE. ATXR5/6 harbor plant homeodomain (PHD) and PCNA-interacting protein (PIP) domains at their N-termini and methyltransferase catalytic SET domain at the C-termini. Y2H assays showed that SE interacts with the SET domain-containing C-termini of the ATXR5/6 proteins (Figures 1B and 1C). Consistent with the Y2H assay, the ATXR5 isoform (ATXR5Δ PIP) that lacks the PIP motif due to alternative splicing was also associated with SE in the co-IP assay, suggesting that PIP domain is dispensable for the SE-ATXR5 interaction (Figure 1D). On the other hand, SE (702 aa) protein comprises a core domain (194–543 aa) containing zinc-finger (ZnF) motif with a walking man-like topology, flanked by two large unstructured regions at the N- and C-termini. The C-terminus harbors a highly

Negative control, pGAD/pGBK vectors. In (D), constructs harboring *35S-FM-ATXR5*, *35S-FM-ATXR5ΔPIP,* and *35S-FM-SGS3* or empty vector were co-infiltrated with *35S-3HA-SE*. IP was conducted by an anti-Myc antibody. Western blot analyses were done using anti-Myc, -HA, or -Actin antibodies to detect the indicated proteins in the Input and IP products. ACTIN and FM-SGS3 served as negative controls. In (E), co-IP was conducted with protein extracts from $P_{ATXR5}$-*FM-ATXR5* transgenic seedlings and Col-0 plants using an anti-Flag antibody. Coimmunoprecipitated protein was detected with the SE-specific antibody (Figure S1E). In (F), MBP-tagged bait proteins and His-Sumo-SE were mixed and pulled down using amylose resin. The recovered MBP-tagged bait proteins were monitored by Coomassie blue staining. The output of the His-tagged prey proteins was analyzed by western blot analysis using a monoclonal anti-His antibody.
(G) Schematic diagram of the full-length and truncated versions of SE used in the Y2H assay. ZnF, zinc finger; CR, conserved region.
(H) Y2H assays show that ATXR5 interacts with the C-terminus of SE protein. Positive control, pGADT7-ATXR5 and pGBKT7-SE full length.
See also Figure S1.

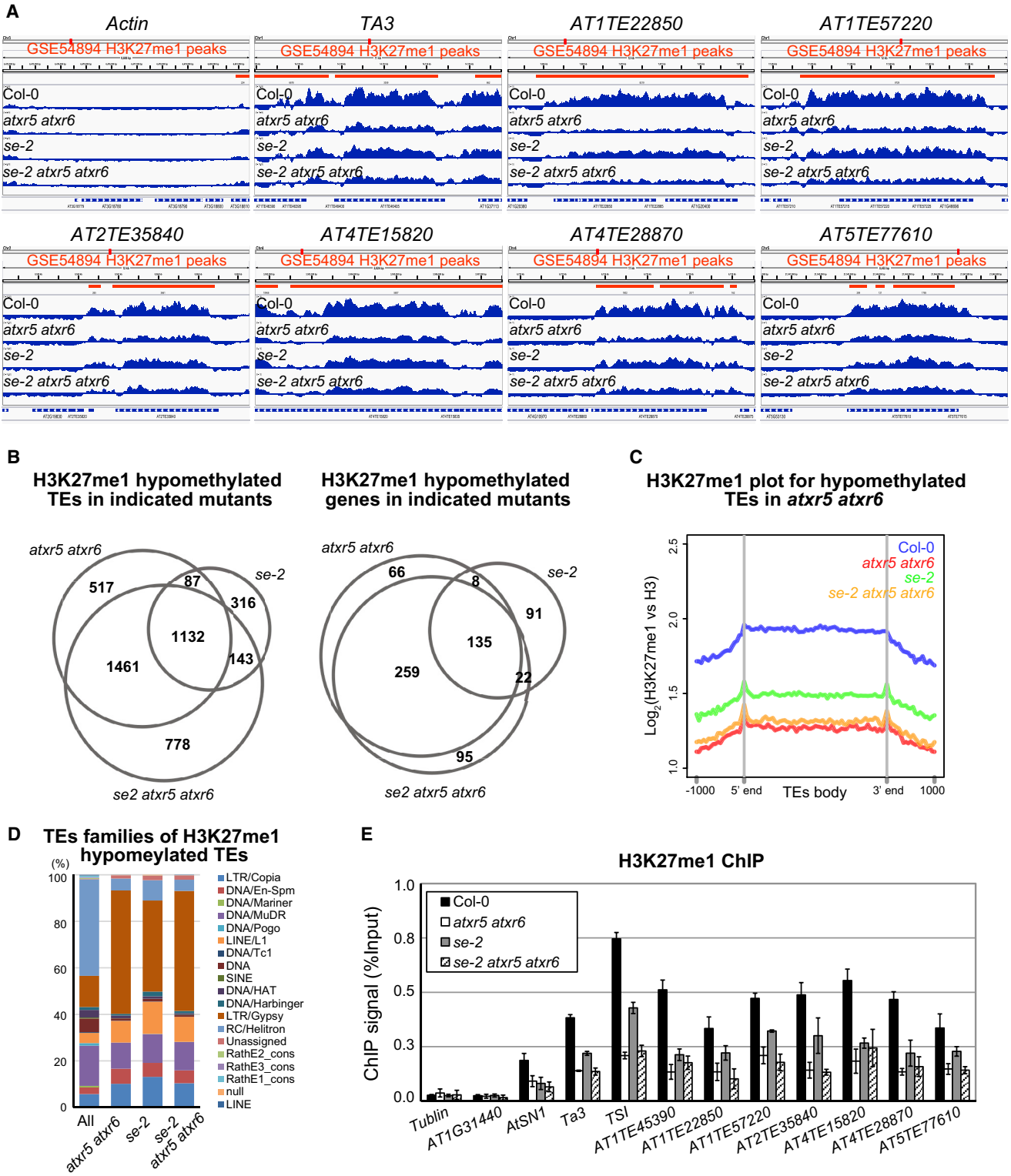


**Figure 2. SE Promotes H3K27me1 Mark in TEs**

(A) ChIP-seq shows that normalized H3K27me1 counts were significantly reduced on exemplified TE loci. TE names and chromosome coordinates are shown on top of each panel. H3K27me1 peaks, which are identified by published data (GSE54894, orange) and recovered in Col-0 and indicated mutants, are shown in blue. Actin serves as a negative control.

(B) Venn diagrams show the overlap of H3K27me1 hypomethylated transposons in the indicated mutants.

(legend continued on next page)

conserved and functionally important but yet uncharacterized sequence (Figure 1G) (Wang et al., 2018). When the C-terminal unstructured domain (642–702 aa) was deleted, the SE-ATXR5 interaction was completely abolished. More precisely, the conserved region (642–695 aa) was sufficient to mediate the interaction between SE and ATXR5 in yeast (Figure 1H). Thus, we conclude that the distal C-terminus of SE interacts with the SET domain containing part of ATXR5.

## SE Promotes H3K27me1 Deposition on Transposons

We initially hypothesized that ATXR5/6 affects the functions of SE-mediated RNA metabolism. However, this possibility was excluded as *atxr5 atxr6* lacked the *se* mutant-characteristic defects in miRNA biogenesis and alternative splicing (Laubinger et al., 2008) (Figure S2; Tables S1 and S2). Next, we hypothesized that SE might participate in ATXR5/6-regulated epigenetic silencing. To test this, we performed the genome-wide H3K27me1 chromatin immunoprecipitation sequencing (ChIP-seq) analysis. We recovered 7,651 genomic regions where H3K27me1 occupancy was significantly decreased in the *atxr5 atxr6* mutant. Of those, 5,884 were overlapped with 3,197 TEs, whereas 837 covered 468 genes (Figures 2A and S2G, Table S3). Notably, among the H3K27me1 hypomethylated regions, 6843 (~89%) were also recovered by an independent H3K27me1 ChIP-seq analysis (Willing et al., 2015). Our ChIP-seq results were also consistent with previous reports (Jacob et al., 2009, 2010), and thus, the datasets are reliable and physiologically relevant.

Interestingly, we recovered a large number of H3K27me1 hypomethylated regions in *se-2* and *se-2 atxr5 atxr6* triple mutants (Figure S2G). These included 1,678 TEs and 256 genes in the *se-2* mutant and 3,514 TEs and 511 genes in the *se-2 atxr5 atxr6* mutant, respectively (Table S3). Comparative analyses revealed that ~73% and ~74% of the H3K27me1 hypomethylated TEs in *se-2* and *se-2 atxr5 atxr6* mutants overlapped with those in the *atxr5 atxr6* mutant, respectively (Figure 2B, Table S3). On the other hand, among 3,197 hypomethylated TEs in the *atxr5 axtr6* mutant, ~38% and ~81% overlapped with those in *se-2* and *se-2 atxr5 axtr6* mutants, respectively. The overlap between the hypomethylated TEs in *atxr5 axtr6* and *se-2* mutants is statistically significant (1,219 overlapped TEs; Log[p] = −2,190.541; hypergeometric test). In total, 1,132 H3K27me1 hypomethylated TEs were shared by *se-2*, *atxr5 atxr6*, and *se-2 atxr5 atxr6* mutants (Figure 2B). In addition to the TEs, significant overlapping of H3K27me1 hypomethylated regions was also found for the protein-coding genes among these mutants (Figure 2B). Next, we focused on the 3,197 hypomethylated TEs in the *atxr5 atxr6* mutant, and plotted H3K27me1 signal for TE bodies with 1-kilobase pairs (kb) upstream and downstream flanking regions. Remarkably, the H3K27me1 signal was also reduced for the ATXR5/6-regulated loci in the *se-2* mutant, but to a lesser extent when compared with that in the *atxr5 atxr6* mutant. No synergistic effect of the H3K27me1 depletion was observed in the *se-2 atxr5 atxr6* mutant (Figures 2C and S2G). Together, these results indicate a substantial overlap between ATXR5/6 and SE-regulated H3K27me1 loci.

TEs can be further divided into different classes. Among them, LTR/Gypsy type TEs are predominantly regulated by ATXR5/6, whereas LTR/Copia and LINE/L1 are regulated through H3K9me2 and non-CG DNA methylation pathways that involve the histone methyltransferases Su(var)3–9 homolog (SUVH)4, SUVH5, SUVH6, and CHROMOMETHYLASE3 (CMT3) (Stroud et al., 2012). In our experiments, the hypomethylated TEs in *se-2* and *se-2 atxr5 atxr6* mutants were over-represented in the LTR/Gypsy family, as also observed in the *atxr5 atxr6* mutant (Figure 2D). These results suggest that SE affects the same type of TE targets that are regulated by ATXR5/6 but not by the non-CG DNA methylation or H3K9me2 pathways.

To validate the H3K27me1 hypomethylation on target TEs, we conducted ChIP-qPCR assays with 10 TE loci, including some previously reported ATXR5/6-regulated ones (Jacob et al., 2010) and several newly identified hypomethylated TEs in the *atxr5 atxr6* mutant from the ChIP-seq assay (Figure 2E). Consistently, the H3K27me1 levels of the tested TEs were decreased in the *atxr5 atxr6* mutant. Notably, although some of the loci were not recovered as hypomethylation TEs in the *se-2* mutant from our ChIP-seq data, the H3K27me1 levels of these TEs were decreased in the *se-2* mutant when tested by the more sensitive ChIP-qPCR assay. These results suggest that the effect on the number of H3K27me1 hypomethylation loci by *SE* loss-of-function was likely undervalued in our H3K27me1 ChIP-seq results due to the relatively low sequencing depth. If so, SE probably impacts H3K27me1 methylation of most of the ATXR5/6-regulated loci. Together, our results demonstrate that SE is a positive regulator of ATXR5/6-catalyzed H3K27me1 mark *in vivo*.

## SE Binds to ATXR5/6-Regulated TE Loci

To test whether SE protein bound to the target TE loci *in vivo*, we performed ChIP-qPCR using the *se-2*; $P_{SE}$*-FM-SE* complementation lines (Figure S3A). We initially tested a few TE loci that are hypomethylated in both *atxr5 atxr6* and *se-2* mutants. ChIP-qPCR assays showed that SE was significantly enriched at the tested TE targets but not at the negative control (Figures S3B and S3C). These results indicate that SE protein is indeed enriched at the tested TE loci.

To investigate how SE associates with chromatin globally, we conducted ChIP-seq experiments. Whole genome ChIP-seq resulted in ~24 million reads uniquely mapped to the reference genome and revealed 5,400 significantly enriched peaks for SE protein compared with a control ChIP-seq with Col-0 plants in the nuclear genome (Table S4). These peaks ranged from hundreds to several kilobases (Figure S3D) throughout heterochromatic and euchromatic regions (Figure 3A). Among the

(C) Plotting of normalized ChIP-seq signals of H3K27me1 in the indicated mutants along TE bodies, including 1 kb of flanking upstream and downstream regions; 3,197 TEs that were hypomethylated in the *atxr5 atxr6* mutant were used.

(D) Classification of the hypomethylated TEs in the indicated mutants. The y axis represents the percentage of individual categories.

(E) ChIP-qPCR confirmation of H3K27me1 hypomethylated TEs in the indicated mutants and Col-0. *Tubulin* and *AT1G31440* are negative controls. Error bars indicate standard deviations of three replicates.

See also Figure S2 and Tables S1, S2 and S3.

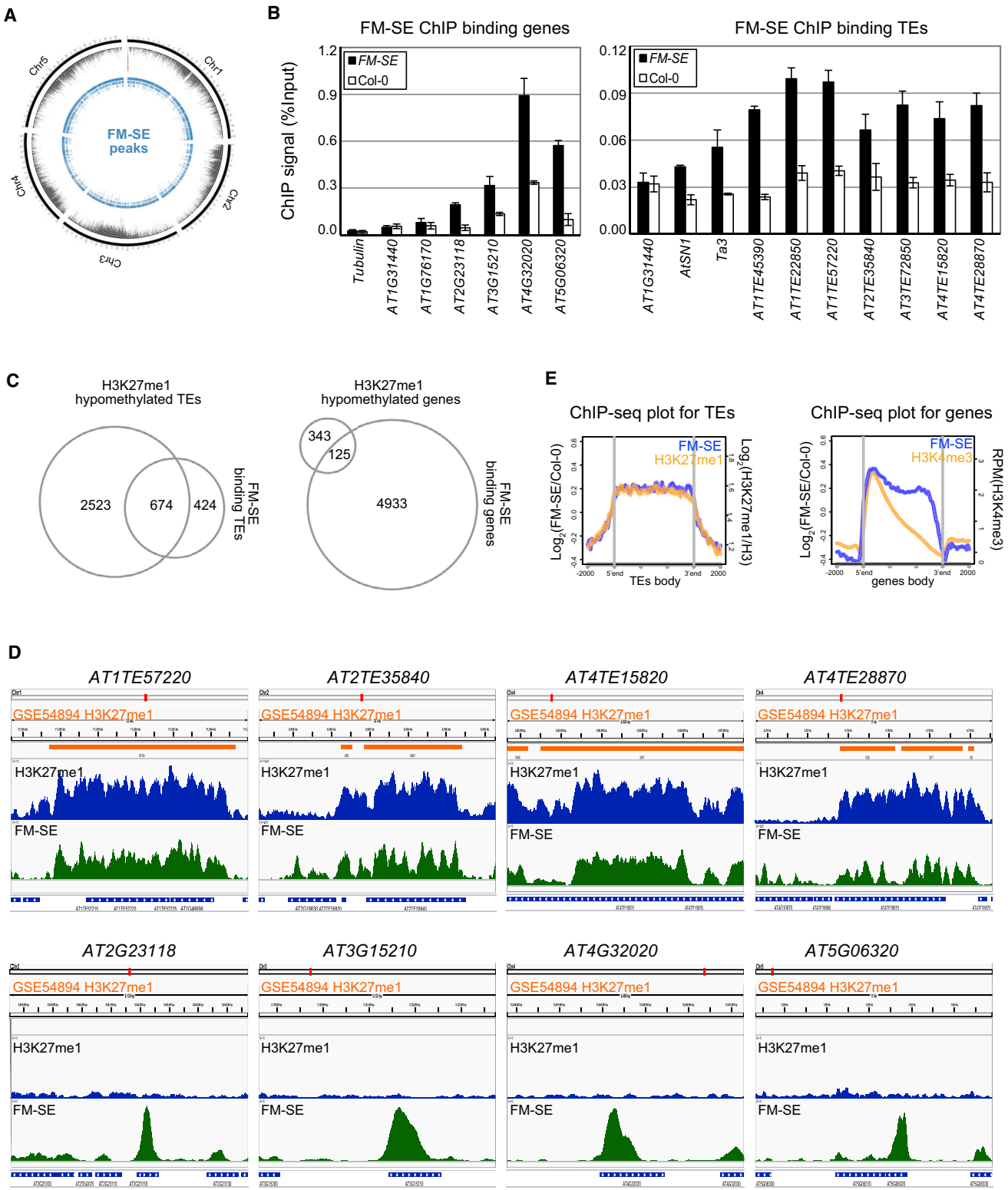


**Figure 3. SE Binds to Targeted TE Loci**

(A) Circos plot shows the genome-wide distribution of FM-SE binding peaks. Outermost to innermost tracks depict *Arabidopsis* chromosome (Chr) 1–5 (ideogram), transposon density (black, histograms), and FM-SE binding peaks (blue, histograms), respectively.

*(legend continued on next page)*

SE-bound peaks, 5,058, 1,098, and 159 loci reside in genes, TEs, and intergenic regions, respectively (Table S4). We selected 14 loci to perform ChIP-qPCR assays. Of those, 13 displayed SE enrichment, indicating the reliability of our ChIP-seq data and suggesting that the identified loci were *bona fide* binding sites of SE *in vivo* (Figure 3B). Next, we compared the SE ChIP peaks of TEs and ATXR5/6-regulated H3K27me1 TE loci. Approximately 61% SE-bound TE loci (674/1,098) overlapped with H3K27me1 hypomethylated TEs detected in the *atxr5 atxr6* mutant. This result represents a significant overlap between SE-bound TE peaks and ATXR5/6-regulated TE loci (Log[p] = −915.5; hypergeometric test). The consistency of SE-bound peaks and H3K27me1 mark in the TE regions is also evident in the Integrative Genomics Viewer (IGV) plot (Figures 3C and 3D).

Interestingly, ATXR5/6-regulated hypomethylated genes also tended to be bound by SE (Log[p] = −14.5; hypergeometric test) (Figure 3C). However, only 125/5,058 of SE-bound protein-coding genes coincided with ATXR5/6-catalyzed H3K27me1 marks. The association of SE with the non-TE loci implied that SE might play a critical role in regulating transcription at these loci. However, the lack of overlap between the SE-bound peaks and H3K27me1 signals in the non-TE loci suggests that the SE-regulatory function at protein-coding gene regions was probably not through the H3K27me1 mark (Figures 3C and 3D).

To further characterize the binding profile of SE in TE and gene bodies, we plotted the SE enrichment signal alongside TEs and protein-coding genes. We observed that the SE binding pattern resembles the distribution profile of H3K27me1 for TEs (Figure 3E), revealing a strong correlation of SE occupancy with H3K27me1 modification at the TE regions *in vivo*. For the protein-coding genes, we used H3K4me3 mark as a reference. Although the SE binding pattern and H3K4me3 profile are distinct, SE is highly enriched at regions proximal to transcription start sites (TSS) (Figures 3D and S3E). This result suggests a regulatory role of SE in transcriptional events at the TSS for protein-coding genes. To investigate whether SE recognizes any consensus DNA sequences, we conducted a motif-searching analysis and found that SE was indeed preferentially associated with numerous motifs (Figure S3F). Notably, these motifs also could be recognized by some other transcription factors from public databases (e.g., ABI4, AP2, and ERF2) (Figure S3F). Such coincidence implies that SE might coordinate with the transcriptional factors to fulfill its regulatory role at the target loci. How SE regulates the non-TE loci at the transcriptional level will be studied elsewhere.

## SE Directly Enhances the ATXR5 Activity

Given that SE promotes ATXR5/6-catalyzed H3K27me1 *in vivo*, we asked whether SE or ATXR5/6 is required for each other's association with the target loci. We generated transgenic plants expressing $P_{SE}$-*FM-SE* in the *se-2* and *se-2 atxr5 atxr6* background and $P_{ATXR5}$-*FM-ATXR5* in the *atxr5* and *se-2 atxr5* background, respectively (Figures S4A and S4B). ChIP-qPCR assays showed that the SE occupancy at the tested TE loci was not decreased in the *atxr5 atxr6* mutant compared with that of the complementation line (Figure S4C). Similarly, the enrichment of ATXR5 was essentially identical in the *se-2* mutant relative to control plants (Figures S4D and S4E). Thus, the occupancy of SE and ATXR5 to the target loci does not depend on each other.

Since SE acts as a scaffold protein to facilitate the assembly of ribonucleoprotein complex to promote RNA processing, we hypothesized that SE could facilitate the supply of H3 substrate to the ATXR5/6 enzymes *in vivo*. To test this, we first conducted *in vitro* pull-down assays and found that SE, like ATXR5, could directly interact with H3 (Figure S4F). We then performed co-IP assays with formaldehyde-cross-linked materials and were able to detect this interaction *in vivo* (Figures S4G and S4H). These results show that both ATXR5 and SE could bind to H3, suggesting that SE might facilitate the access of ATXR5 to the H3 substrate *in vivo*.

Next, we asked whether SE could directly enhance the enzymatic activity of ATXR5/6 *in vitro*. We performed histone methyltransferase (HMTase) assays on calf thymus-histone mixture using the full-length recombinant GST-ATXR5, incubated with His-Sumo, His-Sumo-SE, or His-Sumo-SE C-terminal truncation that does not interact with ATXR5. Incubation of ATXR5 with increasing concentrations of SE augmented the H3K27me1 signal (Figures 4A and 4B). Notably, at a molar ratio of two ATXR5 to one SE, the enzyme activity was doubled, whereas incubation of ATXR5 with the SE truncation did not produce detectable changes. To gain more insight on the mode of action, we performed time course experiments of ATXR5 with either His-Sumo-SE or His-Sumo (Figures 4C and 4D). Consistent with the previous result, incubation of ATXR5 with SE resulted in a larger than 2-fold increase in the H3K27me1 signal, while incubation with His-Sumo had no noticeable effects. Remarkably, while the H3K27me1 signal of ATXR5 control reactions reached their maxima at 30 ∼ 60 min, incubation of ATXR5 with SE continued to increase up to the end of the assay at 90 min. Together, these results indicate that SE directly enhances the activity of ATXR5 *in vitro*.

We also assessed the impact of SE on ATXR6 activity. Notably, the full-length ATXR6 had different substrate preference from ATXR5 (Figure S4I). Consistent with previous studies (Jacob et al., 2009, 2014), ATXR6 had stronger enzymatic activity than ATXR5 on recombinant human H3.1 *in vitro*. But the full-length ATXR6 was not active with the calf thymus-histone mixture, which ATXR5 favored (Figure S4I). We then screened 48 combinations of reaction mixtures and identified an optimal reaction condition, as detected by a strong signal in western blot assays, for ATXR6 (Figure S4J). ATXR6 was incubated

(B) ChIP-qPCR verification of FM-SE binding loci. *Tubulin* and *AT1G31440* serve as negative controls. Error bars indicate standard deviations of three replicates.
(C) Venn diagrams showing the overlapping of the H3K27me1 hypomethylated TEs/genes and the FM-SE binding loci.
(D) IGV view of selected FM-SE ChIP-seq examples. Locus names and chromosome coordinates are shown on top of each panel. Published H3K27me1 peaks (GSE54894, orange), normalized counts of H3K27me1 on target loci in Col-0 (blue), and the signals of FM-SE/control ChIP with Col-0 are shown.
(E) ChIP-seq signals were plotted for TE and gene bodies with 2-kb upstream and downstream flanking regions. Normalized FM-SE/control ChIP with the Col-0 signal (blue); normalized signals of H3K27me1/H3 or normalized H3K4me3 (orange) are shown.
See also Figure S3 and Table S4.

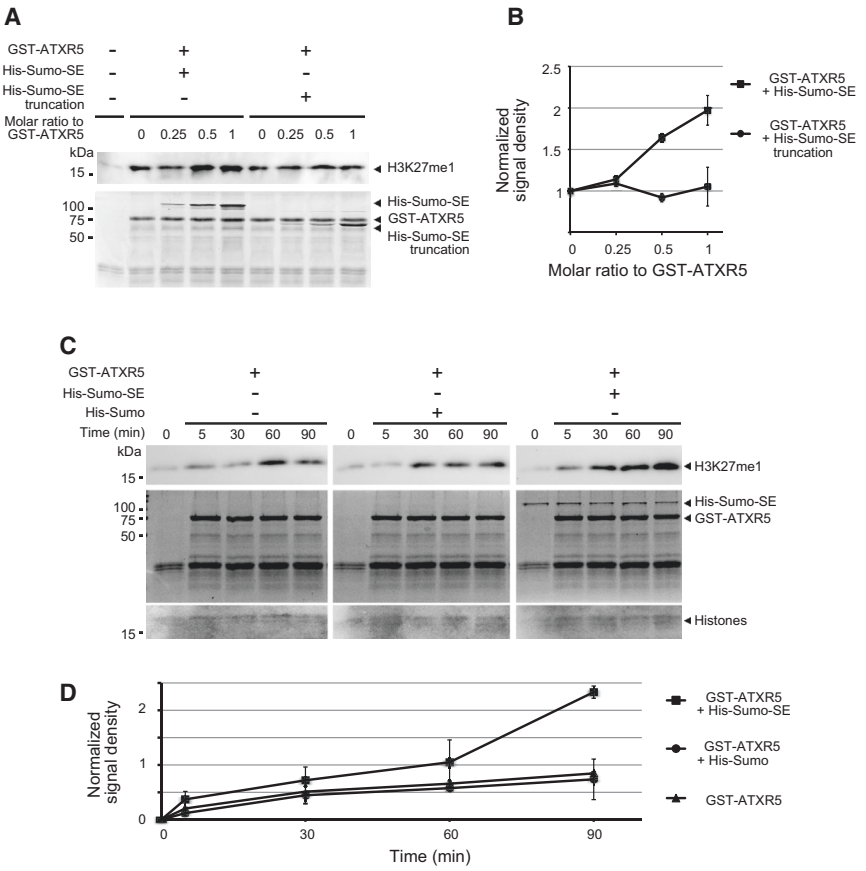


**Figure 4. SE Directly Enhances ATXR5 Activity *In Vitro***

(A) SE enhanced ATXR5 activity in a dose-dependent manner. GST-ATXR5 was incubated with His-Sumo-SE or a His-Sumo-SE C-terminal truncation. Histone mixture from calf thymus was used as the substrate.

(B) Quantitative analysis of ATXR5 activity. The relative intensities of the western blot signals were presented as the mean of three replicates ± standard deviations (SD).

(C) Effect of SE on ATXR5 activity in a time course experiment. GST-ATXR5 was incubated with His-Sumo-SE or His-Sumo and histone mixture from calf thymus was used as the substrate.

(D) Image quantitation of ATXR5 activity in the time course. The relative intensities of western blot signal were presented as the mean of three replicates ±SD ATXR5 activity was analyzed by western blot assay using an anti-H3K27me1 antibody. The proteins in each reaction were monitored by Coomassie blue staining.

See also Figure S4.

with His-Sumo-SE or the control protein, His-Sumo, under the optimal condition. SE only showed marginal enhancement effect on ATXR6 activity (Figure S4K). This effect was not statistically significant, likely because ATXR6 already had strong activity, which might mask the enhancement effect of SE.

## SE Is Required for Transposon Reactivation in the *atxr5 atxr6* Mutant

To investigate whether SE, like ATXR5/6, represses transcription of TEs, we performed RNA sequencing (RNA-seq) analysis of 10-day-old seedlings. Expression levels of *ATXR5/6* and *SE* genes significantly decreased in their corresponding mutants, indicating the reliable quality of our RNA-seq data (Figure S5A; Table S5). Notably, the transcript accumulation of *ATXR5/6* was not affected in the *se-2* mutant, suggesting that the *SE* regulation of *ATXR5/6* function is not through the transcriptional regulation of *ATXR5/6* genes (Figure S5A). RNA-seq analysis showed that the *se* mutation caused 4,189 differentially expressed loci; among these, 2,207 were upregulated, whereas 1,982 downregulated (Figure 5A). The comparable numbers of up or downregulated loci suggests that SE could function as both negative and positive regulators for transcription, depending on biological contexts. Notably, *cbp80* and *hyl1* shared a large portion of co-regulated loci with *se-2*, whereas each mutant had its own specific regulated loci (Figure S5B). Our results were consistent with the fact that SE is involved in pre-mRNA processing, which requires CBC, and in miRNA biogenesis, which entails both CBC and HYL1 (Figures S5B and S2).

Among the 2,207 upregulated loci in the *se-2* mutant, only 34 were TEs. The significantly underrepresented ratio of the reactivated TE loci relative to a large number of H3K27me1 hypomethylation loci was reminiscent of the scenario previously observed in the *atxr5 atxr6* mutant (Stroud et al., 2012). Only 111 of the 3,197 hypomethylated TEs (~3.5%) in *atxr5 atxr6* were also transcriptionally reactivated. This result suggests that the loss-of-function mutations in *SE* and *atxr5 atxr6* had negligible effects on expression of the H3K27me1 hypomethylated TE loci (Figure 5B, Table S5). One explanation could be that H3K27me1 is not the only repressive mark on the TEs and other TGS pathways probably mask the regulatory roles of SE and ATXR5/6 at those loci. In line with this, the introduction of mutations involved in other TGS pathways greatly increases the number of reactivated TEs regulated by H3K27me1 mark (Figure S5C) (Stroud et al., 2012).

To our surprise, there was barely any overlapping between SE- and ATXR5/6-repressed loci except for a few well-characterized TEs (Figures 5B, 5C, S5D, S5E, and S5F). Moreover, the introduction of *se* mutation in the *atxr5 atxr6* background did not have synergistic effect on expression levels of the H3K27me1 hypomethylated TEs. Rather, approximately 60% of 111 TE loci, which were reactivated in the *atxr5 atxr6* mutant, were suppressed in the *se-2 atxr5 atxr6* triple mutant. This suppression was less obvious in the *hyl1 atxr5 atxr6* mutant (Figures 5D and 5E). Consistent with the concerted effect of *SE* and *cbp80* on genome-wide transcription, the introduction of a *cbp80* mutation in the *atxr5 atxr6* background could also suppress *atxr5/6*-reactivated loci (Figures 5D and 5E). Moreover, the significantly suppressed TE loci in *se-2 atxr5 atxr6* and *cbp80 atxr5 atxr6* largely belonged to LTR/Gypsy retrotransposon family with a small percentage of DNA/En-Spm DNA transposon family (Figure 5E). Importantly, the SE protein level was largely reduced in *cbp80*; thus, the regulatory effect of *cbp80* loss-of-function

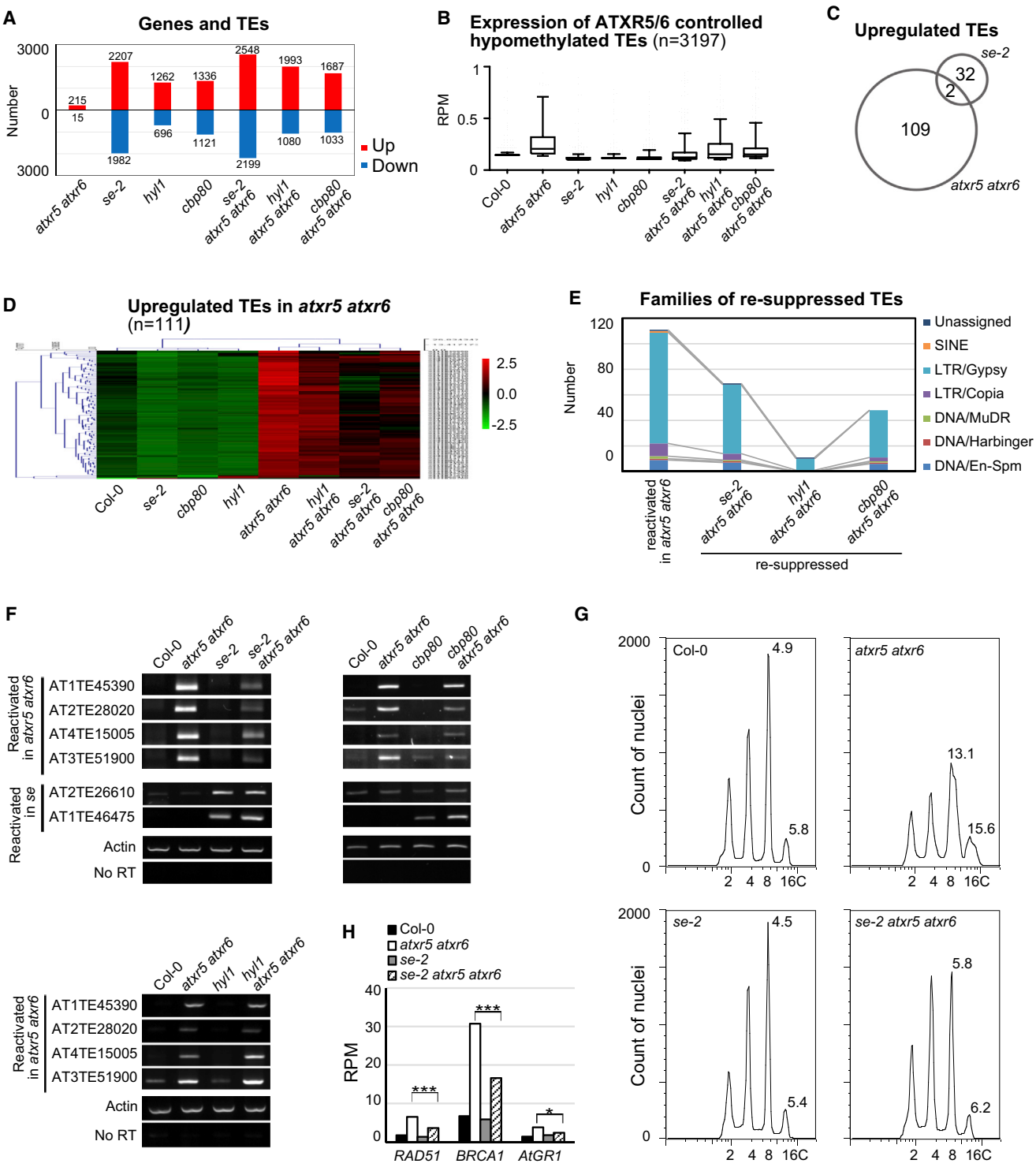


**Figure 5. SE Is Required for the Reactivation of Transposons and Heterochromatic DNA Re-replication Regulated by ATXR5/6**

(A) Numbers of differentially expressed genes and TEs in the indicated mutants compared to Col-0.

(B) Boxplot of RNA-seq reads per million (RPM) values in Col-0 and indicated mutants; 3,197 TEs that were hypomethylated in the *atxr5 atxr6* mutant were used. The line in the middle of the box is plotted at the median. The whiskers are drawn from 10th to 90th percentiles.

(C) Overlap of transcriptionally upregulated TEs in the indicated mutants.

(D) Clustered heatmap of TE expression level in Col-0 and the indicated mutants. 111 TEs, which were significantly upregulated in the *atxr5 atxr6* mutant compared with Col-0 identified by RNA-seq, were clustered according to the $Log_2$RPM value in individual samples. The value was scaled by row and sorted by complete linkage hierarchical clustering with Euclidean distance for samples and TEs.

*(legend continued on next page)*

mutation on gene expression might be partially explained through destabilization of SE protein (Figure S5G).

To further confirm the RNA-seq results, a few loci were selected and verified by RT-PCR assays. Indeed, the TEs reactivated in *atxr5 atxr6* were substantially suppressed in the *se-2 atxr5 atxr6* mutant and to a lesser extent in the *cbp80 atxr5 atxr6* mutant, whereas no obvious repression effect was found in the *hyl1 atxr5 atxr6* mutant. Notably, the long rRNA gene variant reactivated in the *atxr5 atxr6* mutant (Pontvianne et al., 2012) was also repressed by the *se* mutation, implying a general repression effect of the *se* mutation on *ATXR5/6*-regulated transcripts (Figure S5H). On the other hand, the reactivated TEs identified in *SE* were not affected by ATXR5/6 (Figure 5F), suggesting that SE could be involved in other pathways to regulate the expression of these TE loci. Together, these results demonstrate that SE and CBP80 are required for the TE reactivation in *atxr5 atxr6*.

## SE Is Required for Heterochromatic DNA Re-replication in the *atxr5 atxr6* Mutant

ATXR5/6 promote genome stability by suppressing the DNA re-replication phenotype characterized as the accumulation of excess DNA from heterochromatin regions (Jacob et al., 2010, 2014). To test whether SE was also involved in DNA re-replication regulation, we analyzed DNA content of 4-week-old leaf nuclei from different backgrounds by flow cytometry. Consistent with previous reports (Jacob et al., 2010), the 8C and 16C peaks were much broader, as represented by the higher robust CV values in the *atxr5 atxr6* mutant, suggesting an increase in DNA content. By contrast, no obvious DNA re-replication defects were found in the *se-2* mutant because the robust CV values of 8C and 16C peaks in the *se-2* mutant were similar to those of Col-0 (Figure 5G). Notably, the DNA re-replication was suppressed in the *se-2 atxr5 atxr6* triple mutant as compared with the *atxr5 atxr6* mutant (Figure 5G). We also measured the expression levels of several marker genes involved in the homologous recombination (HR) pathway that are upregulated in the *atxr5 atxr6* mutant. In agreement with the DNA re-replication defect, the tested HR genes were upregulated in the *atxr5 atxr6* mutant, while these genes showed no obvious change in the *se-2* mutant. Furthermore, consistent with the suppression of re-replication in the *se-2 atxr5 atxr6* mutant, the expression of the tested HR genes also displayed a significant decrease in the *se-2 atxr5 atxr6* mutant compared with that in the *atxr5 atxr6* mutant (Figure 5H). It has been reported that mutations involved in DNA methylation, nucleosome assembly, and gene expression/RNA export also cause significant suppression of DNA re-replication in the *atxr5 atxr6* mutant (Stroud et al., 2012; Jacob et al., 2014; Hale et al., 2016). However, expression levels of these reported suppressors were not decreased in the *se* mutant (Figure S5A), suggesting the suppression of DNA re-replication by *se* mutation is not through these reported genes. In summary, SE is not only required for the TE reactivation, but also essential for the DNA re-replication in the *atxr5 atxr6* mutant. How *se* mutation suppresses the *atxr5 atxr6*-associated DNA re-replication phenotype will be the focus of future studies.

## Suppression of TE Reactivation by *se* Mutation in the *atxr5 atxr6* Mutant Is Not through DNA Methylation or H3K9me2 Pathways

Previous reports show that non-CG DNA methylation and H3K9me2 mutants could largely alter the expression of *atxr5 atxr6*-reactivated TE loci (Stroud et al., 2012). Moreover, H3K27me1 levels of some TE loci are also decreased in DNA hypomethylation and nucleosome assembly defect mutants (Jacob et al., 2014; Wierzbicki et al., 2008). To test whether *se-2* suppression of *atxr5/6*-reactivated loci involves DNA methylation, we examined DNA methylation levels of representative loci in the *se* mutant with a *drm1 drm2 cmt3* mutant as a positive control. Chop-PCR, locus-specific bisulfate sequencing, and Southern blot analysis all showed that the *se-2* mutation did not cause significant changes in the DNA methylation status of the tested loci (Figures S6A–S6C). We also performed whole genome bisulfite sequencing (WGBS) in *se-2* and related triple mutants. Unlike *met1* and *cmt3 met1* mutants, the *se-2* mutant did not display obvious changes in genome-wide DNA methylation in CG, CHG, and CHH contexts (Figure S6D). We further analyzed the subgroup of H3K27me1 hypomethylated TEs that were shared by *atxr5 atxr6*, *se-2,* and *se-2 atxr5 atxr6* mutants as well as the TEs that were suppressed in the *se-2 atxr5 atxr6* mutant. Such analysis did not reveal a significant difference in DNA methylation levels among the tested mutants (Figures 6A, 6B, and S6E). Thus, the H3K27me1 hypomethylation and suppression of *atxr5/6*-reactivated loci in the *se-2* mutant were not through DNA methylation defect.

In *Arabidopsis*, non-CG DNA methylation is generally correlated with H3K9me2 marks. The tight coordination results from a self-enforcing loop consisting of H3K9me2 histone methyltransferase, Su(var)3–9 homolog 4/Kryptonite (SUVH4/KYP), CMT3, and CMT2 (Du et al., 2015; Stroud et al., 2014). To investigate whether *se* mutation affects H3K9me2 levels, we performed genome-wide H3K9me2 ChIP-seq. Consistent with previous reports, H3K9me2 marks were not significantly altered in the *atxr5 atxr6* mutant (Jacob et al., 2010). In contrast to the positive control *kyp*, H3K9me2 levels were not affected in *se-2* and *se-2 atxr5 atxr6* mutants genome-widely; nor in the loci that were reactivated by *atxr5 atxr6* mutations but suppressed by *se* mutation (Figures 6C–6E, S6F, and S6G). Thus, *se* suppression of TE reactivation in the *atxr5 atxr6* mutant unlikely involves DNA methylation or H3K9me2 pathways.

(E) Classification of 111 TEs that were reactivated in the *atxr5 atxr6* mutant but significantly re-suppressed in the indicated triple mutants. The y axis represents the number of re-suppressed TEs in indicated triple mutants.

(F) RT-PCR validation of expression levels of selected TEs in Col-0 and the indicated mutants. *Actin*, with and without RT, served as an internal control.

(G) Flow cytometry profiles of Col, *atxr5 atxr6*, *se-2*, and *se-2 atxr5 atxr6* plants. The y axis represents the number of nuclei. The x axis shows ploidy levels of the nuclei. The numbers above the peaks (robust CV, widths of the peaks) represent the DNA re-replication levels.

(H) Normalized expression levels of DNA repair genes in the indicated mutants from RNA-seq data. The y axis represents the number of RPMs. ***$q < 0.001$; *$q < 0.05$.

See also Figure S5 and Table S5.

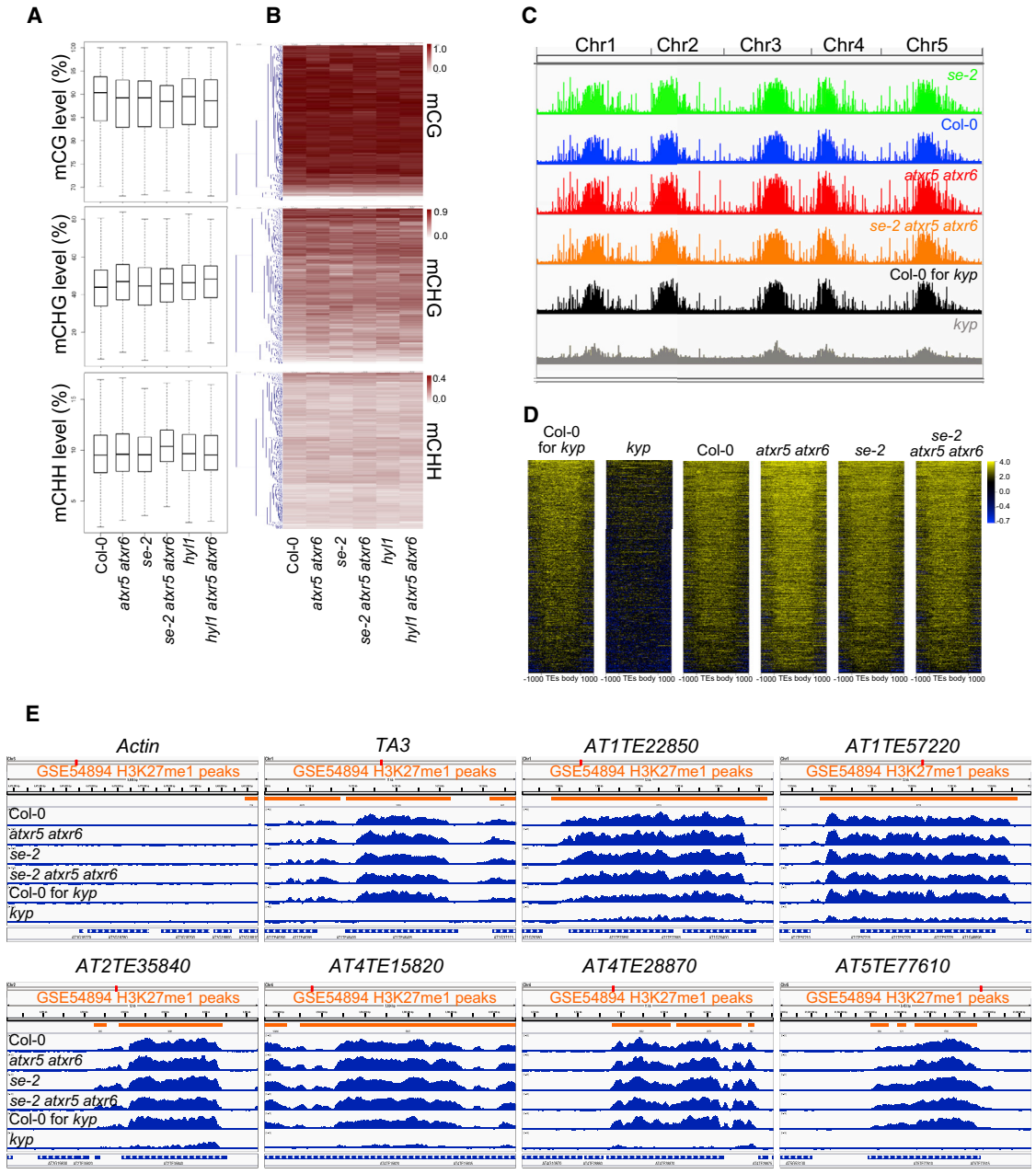


**Figure 6. Regulation of TEs by *se* Mutation Is Not through the DNA Methylation or H3K9me2 Pathways**

(A and B) Box plots (A) and heatmap diagram (B) of CG, CHG, and CHH methylation levels at the 1,132 H3K27me1 hypomethylated TEs shared by *atxr5 atxr6*, *se-2,* and *se-2 atxr5 atxr6* mutants in Col-0 and the indicated mutants. In (B), the rows were sorted by complete linkage hierarchical clustering with Euclidean distance.

(C) Chart diagram of genome-wide H3K9me2 levels in Col-0 and the indicated mutants. The y axis represents normalized reads of H3K9me2 ChIP-seq signal/input DNA for *kyp* and its Col-0 control and the ChIP reads of H3K9me2/H3 for other indicated mutants and their Col-0 control.

(D) Heatmap of H3K9me2 ChIP-seq signals for 1132 H3K27me1 hypomethylated TEs as in (A and B) with 1-kb upstream and downstream flanking regions. ChIP signals of *kyp* and its Col-0 control were normalized to input DNA, whereas the ChIP signals were normalized to H3 for other mutants indicated and their Col-0 control.

(E) Selected TE examples show distribution patterns of H3K9me2 ChIP-seq counts (shown in blue) that were normalized to input for *kyp* and its control and to H3 for the rest lines. Chromosome coordinates and H3K27me1 peaks identified by previously published data (GSE54894, orange) are shown on top of each panel. See also Figure S6.

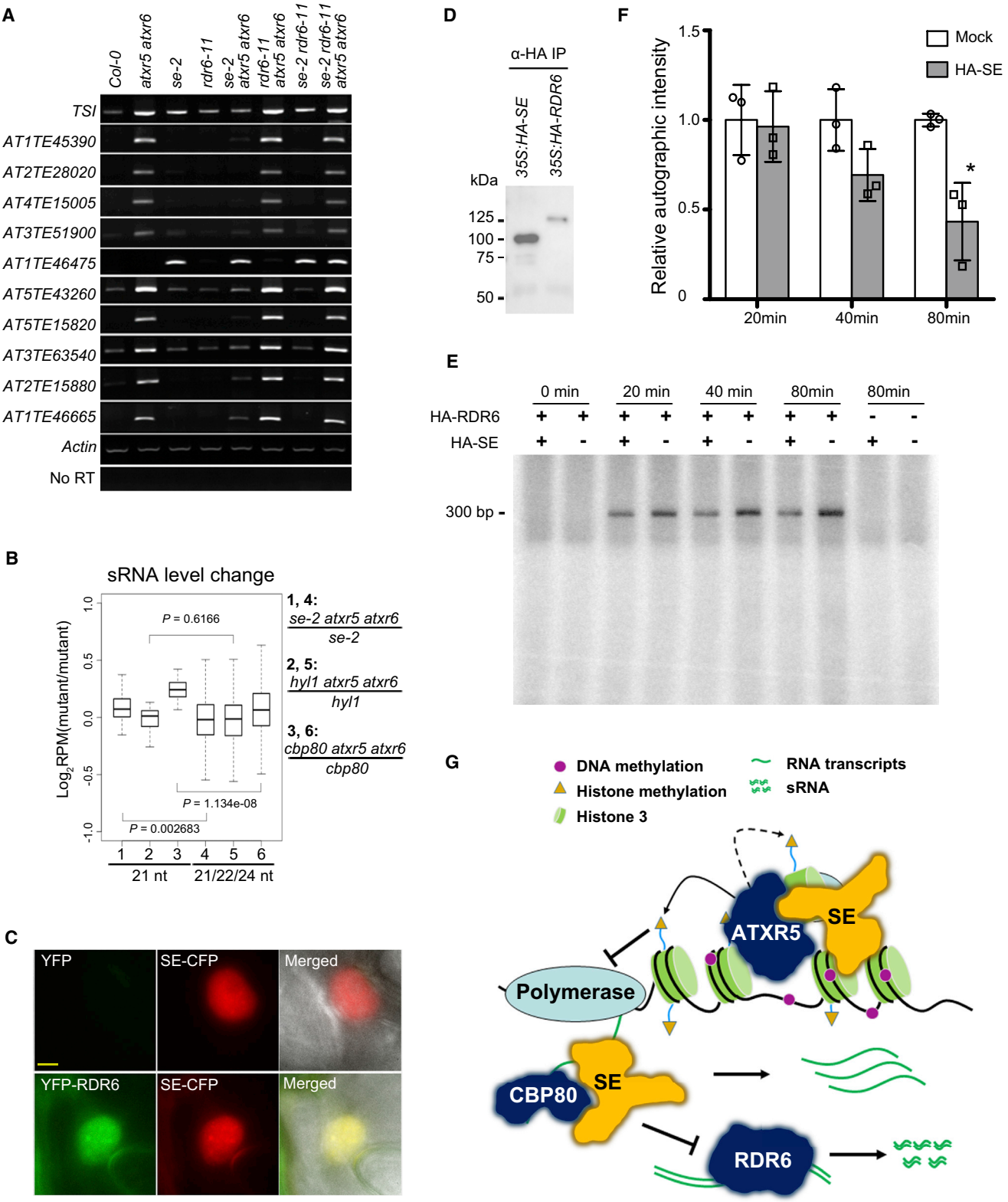


**Figure 7. SE Represses RDR6-Dependent Posttranscriptional Gene Silencing to Protect TE Transcripts**

(A) RT-PCR assays show expression levels of selected TEs in Col-0 and the indicated mutants. *Actin*, with and without RT, served as an internal control.

(B) Changes of 21nt sRNA level in the indicated groups. The y axis represents the $Log_2$RPM of sRNA reads ratio in the indicated groups.

(C) Microscopy image of co-localization of RDR6 with SE in nuclei in *N. benthamiana*. Bar, 5 μM.

*(legend continued on next page)*

### *se* Suppression of *atxr5/6*-Reactivated TEs Is through RDR6

Growing evidence suggests that the RDR6-mediated PTGS pathway could also regulate silencing of TEs in plants (Creasey et al., 2014). The *RDR6* transcript level was not affected in the *se-2* mutant (Figure S5A). We next introduced a *rdr6* mutation into *se-2* and its derived higher-ordered mutants. Interestingly, the TEs that were suppressed in the *se-2 atxr5 atxr6* mutant were restored to the level of the *atxr5 atxr6* mutant in the *rdr6-11 se-2 atxr5 atxr6* quadruple mutant. In contrast, there was not any enhanced expression of the TEs in *rdr6-11 atxr5 atxr6* relative to *atxr5 atxr6* or enhanced expression in *rdr6-11 se-2* relative to *se-2* (Figure 7A). These results suggest that RDR6 is required for the suppression of TEs in the *se-2 atxr5 atxr6* mutant but has a lesser effect on the reactivation of TEs in *atxr5 atxr6* and *se-2* mutants (Figure 7A). As RDR6 is required for the production of secondary siRNAs, we predict that in the absence of SE function, RDR6 activity on the *atxr5/6*-reactivated TEs would result in accumulation of small RNAs (sRNAs) that mapped to these loci. Next, we examined whether there was an increased accumulation of these sRNAs in these mutants by sRNA-seq analyses. Neither the strand distribution nor the profiles of sRNAs that mapped to the target loci were notably different among the tested mutants (Figures S7A and S7B). Interestingly, the enhanced accumulation of RDR6-derived 21 nucleotide (nt) sRNAs that mapped to these TEs in the *se-2 atxr5 atxr6* and *cbp80 atxr5 atxr6* mutants but not in the *hyl1 atxr5 atxr6* mutant was clearly observable at the genome-wide scale, when normalized to their respective single mutants. However, this pattern was not evident for 22nt or 24nt sRNAs (Figure S7C). These results suggest that the increased 21nt-sRNAs are more likely the DCL2/4 processed products, but not the 24nt sRNAs that participate in the RdDM pathway (Figure S7C). Notably, the portion of 21nt sRNAs that mapped to the suppressed TEs in *se-2 atxr5 atxr6* and *cbp80 atxr5 atxr6* as compared to their respective single mutants, was significantly higher than that of the total 21/22/24nt sRNAs. However, this increase was not detected in *hyl1 atxr5 atxr6* as compared to *hyl1* (Figure 7B). These results suggest that the accumulation of these 21nt sRNAs, which processed by the RDR6-DCL2/4 pathways, are repressed by SE and CBP80.

RDR6 is not only a component of the cytosolic PTGS pathway (Kumakura et al., 2009) but also localized in the nucleus and acts on unspliced primary transcripts (Hoffer et al., 2011). Moreover, SE could directly bind to RNA substrates *in vivo* (Raczynska et al., 2014). We hypothesized that SE could compete with RDR6 for the TE transcripts, preventing their processing. To test this hypothesis, we checked the subcellular localization of YFP-RDR6 and SE-CFP in *N. benthamiana*. Although a large portion of the YFP-RDR6 signal is detected in the cytoplasm, a subset of YFP-RDR6 was found in the nucleus. When co-expressed, SE-CFP and YFP-RDR6 clearly overlapped in the nucleus (Figures 7C and S7D). To further investigate whether SE and RDR6 compete for the transcripts, we performed *semi-in vitro* RDR6 enzymatic activity assays as previously described (Curaba and Chen, 2008). We immunoprecipitated HA-RDR6 and HA-SE proteins (Figure 7D), and incubated the proteins with single-stranded RNA (ssRNA) substrates. *Semi-in vitro* assays showed that incubation with SE IP products notably reduced the RDR6 activity, as compared with incubation with IP from mock materials. Moreover, this inhibitory effect was cumulative in time and was statistically significant (Figures 7E and 7F). These results not only indicate that the suppression of TEs in the *se-2 atxr5 atxr6* mutant is dependent on RDR6 but also suggests that SE competes with RDR6. Hence, the TE suppression in *se-2 atxr5 atxr6* is due to the activity of RDR6 on the unprotected TEs transcripts. Taken together, we propose that SE safeguards RNA transcript surveillance by preventing TE transcripts from entry into the RDR6-dependent silencing pathway *in vivo* (Figure 7G).

## DISCUSSION

Here we report a novel function of SE, as it directly associates with the H3K27me1 writers, ATXR5/6, and promotes the accumulation of the ATXR5/6-catalyzed H3K27me1 mark. As such, SE is a positive regulator of transcriptional silencing of the ATXR5/6-regulated loci. On the other hand, this very protein can also antagonize the activity of RDR6 by protecting the TE transcripts from entering the RDR6-dependent PTGS pathway. In this scenario, the normal function of SE will allow the presence of the transcripts by protecting them from the PTGS pathway, while dysfunction or downregulation of SE will result in the channeling of the over-accumulated transcripts to RDR6 and further PTGS pathways for degradation. Thus, the dual roles of SE enable the fine-tuning of the accumulation of TE transcripts in the cell.

How does SE promote the accumulation of ATXR5/6-catalyzed H3K27me1? One possibility is that SE serves as a hub for the supply of the H3 substrate to ATXR5/6 for modification. Two pieces of evidence supported this model: (1) SE could bind to H3 *in vitro* and *in vivo*; and (2) SE could directly promote the ATXR5 activity. Another possibility is that SE could increase the binding affinity of ATXR5 to the cofactors like the methyl-group donor. In addition, SE might serve as a scaffold for the recruitment of yet-unidentified cellular factors to facilitate ATXR5/6 action *in vivo*. For example, it is reported that the enrichment of ASH2R, a core component of H3K4 methyltransferase complexes at specific loci is dependent on the CBC (Li et al., 2016). The mode of action of SE is reminiscent of two scenarios reported in other organisms: in yeast, Ars2 positively regulates H3K9 methylation at the pericentromeric loci and contributes to heterochromatic silencing. Such function of Ars2 appears to be through two interconnected machineries

(D) Western blot analysis of immunoprecipitated HA-tagged RDR6 and SE using anti-HA antibodies.
(E) *Semi-in vitro* assays of RDR6 activity in a time course with and without SE ssRNA substrate and HA-RDR6 were incubated with and without HA-SE with the indicated time points. Signals were detected by phosphor imaging.
(F) Statistics of image quantitation of RDR6 activity. The relative autographic intensities were presented as the mean of three replicates ±SD. *$p < 0.05$.
(G) Working model of dual roles of SE not only promotes ATXR5/6 activity in epigenetic silencing of TEs but also protects TE transcripts from RDR6 activity to attenuate RNA silencing effect.
See also Figure S7.

called Red1-containing nuclear RNA silencing (NURS) and Clr4–Rik1–Cul4 (CLRC) methyltransferase complexes that catalyze H3K9me2/3 to initiate heterochromatin formation (Egan et al., 2014). In the other scenario, Ars2 cooperates with carbon catabolite repressor 4 (CCR4) Ccr4-NOT complex, in addition to the Red1-containing core complex, to promote meiotic mRNA decay and facultative heterochromatin assembly at retrotransposons and at developmentally regulated genes (Sugiyama et al., 2016). However, there are some fundamental differences between SE and Pir2/Ars2 functions in the TGS: first, Pir2/Ars2 targets H3K9 methyltransferase in yeast and mammals, whereas SE acts on H3K27me1 writers in *Arabidopsis*. Moreover, the SE promotion of ATXR5/6-catalyzed H3K27me1 might be specific, as SE appears not to interact with SUVH4/KYP (data not shown), which deposits H3K9me2/3, or with PRC2 components, which catalyze H3K27me2/3 in plants. Second, Pir2/Ars2 participation in epigenetic silencing engages in an RNAi-dependent process. However, SE promotion of ATXR5/6 activity in plants does not appear to involve the DNA methylation or H3K9me2 pathways. The precise mechanism of how SE promotes ATXR5/6 activity awaits future crystal or Cyro-EM structure analysis.

Although *se* mutation causes genome-wide reduction of H3K27me1, this reduction does not cause genome-wide reactivation of TEs as well as DNA re-replication as observed in the *atxr5 atxr6* mutant (Figure 5). We proposed several non-exclusive hypotheses: first, there might be a threshold of H3K27me1 depletion for triggering TE reactivation and DNA re-replication. The *se* mutant has less severe H3K27me1 defect relative to *atxr5 atxr6*, and might not reach the threshold to induce the other two phenotypes (Figures 2C and S2G). Second, ATXR5/6-regulated TEs are probably controlled by multiple silencing machineries, and downregulation of the H3K27me1 mark itself is probably insufficient to release their expression, or its effects are masked by other epigenetic events. Compared with the large number of hypomethylated TEs, only a small subset of TEs was reactivated even in the *atxr5 atxr6* mutant. A similar scenario is observed when a change of repressive marks such as H3K9me2 does not correlate with transcriptional changes at the targeted loci (Egan et al., 2014). Relative to the *atxr5 atxr6* mutant, many more reactivated TEs are detected in the triple mutants of *atxr5 atxr6* with DNA methylation-deficient mutants (Figure S5). Here, SE is a multifunctional protein that might also be involved in other TGS/PTGS pathways, leading to a low extent of TE reactivation in the *se* mutant. In addition to the positive regulation of H3K27me1, SE might fulfill other functions that counter the silencing of ATXR5/6-regulated loci. Such function is actually highlighted in the *se-2 atxr5 atxr6* triple mutant where the TEs and DNA re-replication have been suppressed.

*se* mutation suppresses reactivation of TEs in *atxr5 axtr6* but not in *rdr6 atxr5 axtr6* (Figure 7). Such result indicates that the suppression of ATXR5/6-regulated TEs in the absence of SE is clearly caused by RDR6 activity. Several pieces of evidence support this notion: (1) expression of the TEs repressed in the *se-2 atxr5 axtr6* mutant is reactivated in the *rdr6-11 se-2 atxr5 axtr6* quadruple mutant; (2) a fraction of RDR6 protein is localized to the nucleus, suggesting that RDR6 has uncharacterized functions in addition to its canonical activity in cytosol; (3) co-localization of RDR6 and SE suggests the functional connection between the two proteins; and (4) SE and RDR6 compete for the same substrates *in semi-vitro*. One plausible model of how SE suppresses RDR6 function would be that SE inhibits RDR6 activity through its interaction with CBC and the spliceosome. It has been reported that transcripts from transgenes, relative to intron-containing mRNAs, are more effective substrates for RDR6-mediated gene silencing. The intron-based suppression of RNA silencing depends on SE and CBP80, presumably due to their competition for the same substrates (Christie et al., 2011). TE transcripts resemble those from transgenes; thus, they are suitable substrates of RDR6. CBP80 and SE probably bind to the transcripts generated from the ATXR5/6-regulated TE loci, despite their lack of introns. In this scenario, SE/CBP80 might impede the polymerase activity of RDR6 by depleting the pool of available substrates. This would probably explain why both mutations of *se* and *cbp80*, but not *hyl1*, could suppress *atxr5/6*-reactivated loci, although to different extents. Alternatively, SE might coordinate with RNA surveillance factors to suppress RDR6-mediated RNA silencing in *Arabidopsis*. Numerous RNA quality control pathways compete with endogenous RDR activities to deter RNA silencing. This has been exemplified by members of the 5′-3′ XRN exonuclease family (Gy et al., 2007), CCR4 (Moreno et al., 2013), and SKI-containing exosome complex (Zhang et al., 2015), among others (Liu and Chen, 2016), which have been shown to directly compete for RDR6 substrates in *Arabidopsis*. In fact, our proteomics analysis of the SE complex also recovered XRN3, which has been associated with the clearance of debris from pri-miRNA processing in the nucleus; thus, it is plausible that SE cooperates with these RNA quality control factors to impede RDR6 function on TE transcripts in plants (Lee et al., 2013). Of course, SE might couple with yet uncharacterized RNA processing pathways to inhibit RDR6 function. In line with this model, a recent genetic screening for suppressors of ATXR5/6 identified new mutants involved in RNA processing (Hale et al., 2016). Given that these mutants have a similar phenotype as the *se* mutation regarding the suppression of *atxr5/6*-reactivated TEs, they might act in concert with each other to antagonize RDR6 function and attenuate RNA silencing.

In summary, we found that the multifunctional protein SE has a non-canonical role, as a coordinator of ATXR5/6-mediated TGS and RDR6-mediated PTGS silencing of TEs. It should be noted that apart from repressing TE expression, ATXR5/6 also contributes to the maintenance of genome stability (Hale et al., 2016; Jacob et al., 2009, 2010, 2014; Stroud et al., 2012). SE is also a suppressor of the DNA re-replication phenotype in *atxr5 atxr6*. How SE participates in the ATXR5/6-mediated maintenance of genome stability and whether such process is coupled with SE regulation of TE expression awaits future efforts. Furthermore, we noticed that SE is predominantly localized to protein-coding gene regions besides TE loci, but how is SE recruited to the protein-coding genes and whether it regulates the transcription of the targeted loci will also be an exciting research topic.

## STAR★METHODS

Detailed methods are provided in the online version of this paper and include the following:

- KEY RESOURCES TABLE
- CONTACT FOR REAGENT AND RESOURCE SHARING

## SUPPLEMENTAL INFORMATION

Supplemental Information includes seven figures and six tables and can be found with this article online at https://doi.org/10.1016/j.devcel.2018.05.023.

## ACKNOWLEDGMENTS

We thank Drs. S. Michaels, Y. Jacob, R. Martienssen, and X. Chen for their generous sharing of ATXR5/6 and RDR6 plasmids and mutant alleles, Y. Chen and J. Yuan for bioinformatics advice, and L. Zeng and the Microscopy and Imaging Center facility at Texas A&M University for imaging facilities. We also thank T. Flusche for careful proofreading of this manuscript. The work was supported by a grant from NSF (MCB-1716243) to X.Z., D.S., and X.S. were supported by a China Scholar Council fellowship.

## AUTHOR CONTRIBUTIONS

X.Z. conceived the project. Z.M. and X.Z. designed the study. Z.M., C.C.-G., Z.W., X.H., X.S., and D.S. performed the experiments. M.E.P. provided experimental materials and intellectual input. Z.M., C.C.-G., and X.Z. analyzed data and wrote the paper.

## DECLARATION OF INTERESTS

The authors declare no competing interests.

Received: November 19, 2017
Revised: April 4, 2018
Accepted: May 20, 2018
Published: June 18, 2018

## REFERENCES

Andreu-Agullo, C., Maurin, T., Thompson, C.B., and Lai, E.C. (2012). Ars2 maintains neural stem-cell identity through direct transcriptional activation of Sox2. Nature *481*, 195–198.

Cao, X., Aufsatz, W., Zilberman, D., Mette, M.F., Huang, M.S., Matzke, M., and Jacobsen, S.E. (2003). Role of the DRM and CMT3 methyltransferases in RNA-directed DNA methylation. Curr. Biol. *13*, 2212–2217.

Castillo-Gonzalez, C., Liu, X., Huang, C., Zhao, C., Ma, Z., Hu, T., Sun, F., Zhou, Y., Zhou, X., Wang, X.J., et al. (2015). Geminivirus-encoded TrAP suppressor inhibits the histone methyltransferase SUVH4/KYP to counter host defense. Elife *4*, e06671.

Christie, M., Croft, L.J., and Carroll, B.J. (2011). Intron splicing suppresses RNA silencing in *Arabidopsis*. Plant J. *68*, 159–167.

Creasey, K.M., Zhai, J., Borges, F., Van Ex, F., Regulski, M., Meyers, B.C., and Martienssen, R.A. (2014). miRNAs trigger widespread epigenetically activated siRNAs from transposons in *Arabidopsis*. Nature *508*, 411–415.

Curaba, J., and Chen, X. (2008). Biochemical activities of *Arabidopsis* RNA-dependent RNA polymerase 6. J. Biol. Chem. *283*, 3059–3066.

Deal, R.B., and Henikoff, S. (2011). Histone variants and modifications in plant gene regulation. Curr. Opin. Plant Biol. *14*, 116–122.

Du, J.M., Johnson, L.M., Jacobsen, S.E., and Patel, D.J. (2015). DNA methylation pathways and their crosstalk with histone methylation. Nat. Rev. Mol. Cell Biol. *16*, 519–532.

Egan, E.D., Braun, C.R., Gygi, S.P., and Moazed, D. (2014). Post-transcriptional regulation of meiotic genes by a nuclear RNA silencing complex. RNA *20*, 867–881.

Fang, Y., and Spector, D.L. (2007). Identification of nuclear dicing bodies containing proteins for microRNA biogenesis in living arabidopsis plants. Curr. Biol. *17*, 818–823.

Gruber, J.J., Zatechka, D.S., Sabin, L.R., Yong, J., Lum, J.J., Kong, M., Zong, W.X., Zhang, Z., Lau, C.K., Rawlings, J., et al. (2009). Ars2 links the nuclear cap-binding complex to RNA interference and cell proliferation. Cell *138*, 328–339.

Gy, I., Gasciolli, V., Lauressergues, D., Morel, J.B., Gombert, J., Proux, F., Proux, C., Vaucheret, H., and Mallory, A.C. (2007). *Arabidopsis* FIERY1, XRN2, and XRN3 are endogenous RNA silencing suppressors. Plant Cell *19*, 3451–3461.

Hale, C.J., Potok, M.E., Lopez, J., Do, T., Liu, A., Gallego-Bartolome, J., Michaels, S.D., and Jacobsen, S.E. (2016). Identification of multiple proteins coupling transcriptional gene silencing to genome stability in *Arabidopsis thaliana*. PLoS Genet. *12*, e1006092.

Hallais, M., Pontvianne, F., Andersen, P.R., Clerici, M., Lener, D., Benbahouche Nel, H., Gostan, T., Vandermoere, F., Robert, M.C., Cusack, S., et al. (2013). CBC-ARS2 stimulates 3'-end maturation of multiple RNA families and favors cap-proximal processing. Nat. Struct. Mol. Biol. *20*, 1358–1366.

Hoffer, P., Ivashuta, S., Pontes, O., Vitins, A., Pikaard, C., Mroczka, A., Wagner, N., and Voelker, T. (2011). Posttranscriptional gene silencing in nuclei. Proc. Natl. Acad. Sci. USA *108*, 409–414.

Iwasaki, M., and Paszkowski, J. (2014). Epigenetic memory in plants. EMBO J. *33*, 1987–1998.

Jacob, Y., Bergamin, E., Donoghue, M.T.A., Mongeon, V., LeBlanc, C., Voigt, P., Underwood, C.J., Brunzelle, J.S., Michaels, S.D., Reinberg, D., et al. (2014). Selective methylation of histone H3 variant H3.1 regulates heterochromatin replication. Science *343*, 1249–1253.

Jacob, Y., Feng, S., LeBlanc, C.A., Bernatavichute, Y.V., Stroud, H., Cokus, S., Johnson, L.M., Pellegrini, M., Jacobsen, S.E., and Michaels, S.D. (2009). ATXR5 and ATXR6 are H3K27 monomethyltransferases required for chromatin structure and gene silencing. Nat. Struct. Mol. Biol. *16*, 763–768.

Jacob, Y., Stroud, H., Leblanc, C., Feng, S., Zhuo, L., Caro, E., Hassel, C., Gutierrez, C., Michaels, S.D., and Jacobsen, S.E. (2010). Regulation of heterochromatic DNA replication by histone H3 lysine 27 methyltransferases. Nature *466*, 987–991.

Jiao, L., and Liu, X. (2015). Structural basis of histone H3K27 trimethylation by an active polycomb repressive complex 2. Science *350*, aac4383.

Krueger, F., and Andrews, S.R. (2011). Bismark: a flexible aligner and methylation caller for Bisulfite-Seq applications. Bioinformatics *27*, 1571–1572.

Kumakura, N., Takeda, A., Fujioka, Y., Motose, H., Takano, R., and Watanabe, Y. (2009). SGS3 and RDR6 interact and colocalize in cytoplasmic SGS3/RDR6-bodies. FEBS Lett. *583*, 1261–1266.

Langmead, B., Trapnell, C., Pop, M., and Salzberg, S.L. (2009). Ultrafast and memory-efficient alignment of short DNA sequences to the human genome. Genome Biol. *10*, R25.

Laubinger, S., Sachsenberg, T., Zeller, G., Busch, W., Lohmann, J.U., Ratsch, G., and Weigel, D. (2008). Dual roles of the nuclear cap-binding complex and

SERRATE in pre-mRNA splicing and microRNA processing in *Arabidopsis thaliana*. Proc. Natl. Acad. Sci. USA *105*, 8795–8800.

Laubinger, S., Zeller, G., Henz, S.R., Buechel, S., Sachsenberg, T., Wang, J.W., Ratsch, G., and Weigel, D. (2010). Global effects of the small RNA biogenesis machinery on the *Arabidopsis thaliana* transcriptome. Proc. Natl. Acad. Sci. USA *107*, 17466–17473.

Lee, N.N., Chalamcharla, V.R., Reyes-Turcu, F., Mehta, S., Zofall, M., Balachandran, V., Dhakshnamoorthy, J., Taneja, N., Yamanaka, S., Zhou, M., et al. (2013). Mtr4-like protein coordinates nuclear RNA processing for heterochromatin assembly and for telomere maintenance. Cell *155*, 1061–1074.

Li, Z., Jiang, D., Fu, X., Luo, X., Liu, R., and He, Y. (2016). Coupling of histone methylation and RNA processing by the nuclear mRNA cap-binding complex. Nat. Plants *2*, 16015.

Lisch, D. (2013). How important are transposons for plant evolution? Nat. Rev. Genet. *14*, 49–61.

Liu, C., Lu, F., Cui, X., and Cao, X. (2010). Histone methylation in higher plants. Annu. Rev. Plant Biol. *61*, 395–420.

Liu, J., Jung, C., Xu, J., Wang, H., Deng, S., Bernad, L., Arenas-Huertero, C., and Chua, N.H. (2012). Genome-wide analysis uncovers regulation of long intergenic noncoding RNAs in *Arabidopsis*. Plant Cell *24*, 4333–4345.

Liu, L., and Chen, X. (2016). RNA quality control as a key to suppressing RNA silencing of endogenous genes in plants. Mol. Plant *9*, 826–836.

Makarevitch, I., Waters, A.J., West, P.T., Stitzer, M., Hirsch, C.N., Ross-Ibarra, J., and Springer, N.M. (2015). Transposable elements contribute to activation of maize genes in response to abiotic stress. PLoS Genet. *11*, e1004915.

Margueron, R., and Reinberg, D. (2011). The polycomb complex PRC2 and its mark in life. Nature *469*, 343–349.

Matzke, M., and Mosher, R. (2014). RNA-directed DNA methylation: an epigenetic pathway of increasing complexity. Nat. Rev. Genet. *15*, 394–408.

Matzke, M.A., Kanno, T., and Matzke, A.J. (2015). RNA-directed DNA methylation: the evolution of a complex epigenetic pathway in flowering plants. Annu. Rev. Plant Biol. *66*, 243–267.

Moreno, A.B., Martinez de Alba, A.E., Bardou, F., Crespi, M.D., Vaucheret, H., Maizel, A., and Mallory, A.C. (2013). Cytoplasmic and nuclear quality control and turnover of single-stranded RNA modulate post-transcriptional gene silencing in plants. Nucleic Acids Res. *41*, 4699–4708.

Peragine, A., Yoshikawa, M., Wu, G., Albrecht, H.L., and Poethig, R.S. (2004). SGS3 and SGS2/SDE1/RDR6 are required for juvenile development and the production of trans-acting siRNAs in *Arabidopsis*. Genes Dev. *18*, 2368–2379.

Pontvianne, F., Blevins, T., Chandrasekhara, C., Feng, W., Stroud, H., Jacobsen, S.E., Michaels, S.D., and Pikaard, C.S. (2012). Histone methyltransferases regulating rRNA gene dose and dosage control in Arabidopsis. Genes Dev. *26*, 945–957.

Raczynska, K.D., Stepien, A., Kierzkowski, D., Kalak, M., Bajczyk, M., McNicol, J., Simpson, C.G., Szweykowska-Kulinska, Z., Brown, J.W.S., and Jarmolowski, A. (2014). The SERRATE protein is involved in alternative splicing in *Arabidopsis thaliana*. Nucleic Acids Res. *42*, 1224–1244.

Robinson, J.T., Thorvaldsdóttir, H., Winckler, W., Guttman, M., Lander, E.S., Getz, G., and Mesirov, J.P. (2011). Integrative genomics viewer. Nat. Biotechnol. *29*, 24–26.

Robinson, M.D., McCarthy, D.J., and Smyth, G.K. (2010). edgeR: a bioconductor package for differential expression analysis of digital gene expression data. Bioinformatics *26*, 139–140.

Sabin, L.R., Zhou, R., Gruber, J.J., Lukinova, N., Bambina, S., Berman, A., Lau, C.K., Thompson, C.B., and Cherry, S. (2009). Ars2 regulates both miRNA- and siRNA-dependent silencing and suppresses RNA virus infection in *Drosophila*. Cell *138*, 340–351.

Shen, L., Shao, N., Liu, X., and Nestler, E. (2014). ngs.plot: quick mining and visualization of next-generation sequencing data by integrating genomic databases. BMC Genomics *15*, 284.

Sienski, G., Donertas, D., and Brennecke, J. (2012). Transcriptional silencing of transposons by Piwi and maelstrom and its impact on chromatin state and gene expression. Cell *151*, 964–980.

Stroud, H., Hale, C.J., Feng, S., Caro, E., Jacob, Y., Michaels, S.D., and Jacobsen, S.E. (2012). DNA methyltransferases are required to induce heterochromatic re-replication in arabidopsis. PLoS Genet. *8*, e1002808.

Stroud, H., Greenberg, M.V., Feng, S., Bernatavichute, Y.V., and Jacobsen, S.E. (2013). Comprehensive analysis of silencing mutants reveals complex regulation of the Arabidopsis methylome. Cell *152*, 352–364.

Stroud, H., Do, T., Du, J., Zhong, X., Feng, S., Johnson, L., Patel, D.J., and Jacobsen, S.E. (2014). Non-CG methylation patterns shape the epigenetic landscape in *Arabidopsis*. Nat. Struct. Mol. Biol. *21*, 64–72.

Sugiyama, T., Thillainadesan, G., Chalamcharla, V.R., Meng, Z., Balachandran, V., Dhakshnamoorthy, J., Zhou, M., and Grewal, S.I. (2016). Enhancer of rudimentary cooperates with conserved RNA-processing factors to promote meiotic mRNA decay and facultative heterochromatin assembly. Mol. Cell *61*, 747–759.

Tan, M.J., Luo, H., Lee, S., Jin, F.L., Yang, J.S., Montellier, E., Buchou, T., Cheng, Z.Y., Rousseaux, S., Rajagopal, N., et al. (2011). Identification of 67 histone marks and histone lysine crotonylation as a new type of histone modification. Cell *146*, 1015–1027.

Trapnell, C., Pachter, L., and Salzberg, S.L. (2009). TopHat: discovering splice junctions with RNA-Seq. Bioinformatics *25*, 1105–1111.

Wang, Z., Li, X., Jiang, Y., Shao, Q., Liu, Q., Chen, B., and Huang, D. (2015). swDMR: a sliding window approach to identify differentially methylated regions based on whole genome bisulfite sequencing. PLoS One *10*, e0132866.

Wang, Z., Ma, Z., Castillo-González, C., Sun, D., Li, Y., Yu, B., Zhao, B., Li, P., and Zhang, X. (2018). SWI2/SNF2 ATPase CHR2 remodels pri-miRNAs via SE to impede miRNA production. Nature. . Published online May 16, 2018. https://doi.org/10.1038/s41586-018-0135-x.

Wierzbicki, A.T., Haag, J.R., and Pikaard, C.S. (2008). Noncoding transcription by RNA polymerase Pol IVb/Pol V mediates transcriptional silencing of overlapping and adjacent genes. Cell *135*, 635–648.

Willing, E.-M., Rawat, V., Mandáková, T., Maumus, F., James, G.V., Nordström, K.J.V., Becker, C., Warthmann, N., Chica, C., Szarzynska, B., et al. (2015). Genome expansion of *Arabis alpina* linked with retrotransposition and reduced symmetric DNA methylation. Nat. Plants *1*, 14023.

Yang, L., Liu, Z., Lu, F., Dong, A., and Huang, H. (2006). SERRATE is a novel nuclear regulator in primary microRNA processing in *Arabidopsis*. Plant J. *47*, 841–850.

Zhang, X., Garreton, V., and Chua, N.H. (2005). The AIP2 E3 ligase acts as a novel negative regulator of ABA signaling by promoting ABI3 degradation. Genes Dev. *19*, 1532–1543.

Zhang, X., Yuan, Y.R., Pei, Y., Lin, S.S., Tuschl, T., Patel, D.J., and Chua, N.H. (2006). Cucumber mosaic virus-encoded 2b suppressor inhibits *Arabidopsis* Argonaute1 cleavage activity to counter plant defense. Genes Dev. *20*, 3255–3268.

Zhang, X., Zhu, Y., Liu, X., Hong, X., Xu, Y., Zhu, P., Shen, Y., Wu, H., Ji, Y., Wen, X., et al. (2015). Suppression of endogenous gene silencing by bidirectional cytoplasmic RNA decay in *Arabidopsis*. Science *348*, 120–123.

Zhang, Y., Liu, T., Meyer, C.A., Eeckhoute, J., Johnson, D.S., Bernstein, B.E., Nusbaum, C., Myers, R.M., Brown, M., Li, W., et al. (2008). Model-based analysis of ChIP-seq (MACS). Genome Biol. *9*, R137.

Zhu, H., Hu, F., Wang, R., Zhou, X., Sze, S.H., Liou, L.W., Barefoot, A., Dickman, M., and Zhang, X. (2011). *Arabidopsis* Argonaute10 specifically sequesters miR166/165 to regulate shoot apical meristem development. Cell *145*, 242–256.

Zhu, H., Zhou, Y., Castillo-Gonzalez, C., Lu, A., Ge, C., Zhao, Y.T., Duan, L., Li, Z., Axtell, M.J., Wang, X.J., et al. (2013). Bidirectional processing of pri-miRNAs with branched terminal loops by *Arabidopsis* Dicer-like1. Nat. Struct. Mol. Biol. *20*, 1106–1115.